Research Article Vol. 9, No. 3 / March 2021 / Photonics Research 351

PHOTONICS Research

Solution-processed lead-free bulk 0D $Cs_3Cu_2I_5$ single crystal for indirect gamma-ray spectroscopy application

Qiang Xu,[1,*] Juan Wang,[1] Qindong Zhang,[1] Xiao Ouyang,[2,3] Maheng Ye,[1] Weiting Xie,[4] Xuewen Yan,[4] Deyuan Li,[4] Xiaoping Ouyang,[2,3,5] Xiaobing Tang,[1] and Xiaodong Zhang[4]

[1]Department of Nuclear Science and Engineering, Nanjing University of Aeronautics and Astronautics, Nanjing 211106, China
[2]Shaanxi Engineering Research Center of Controllable Neutron Source, School of Science, Xijing University, Xi'an 710123, China
[3]Institute of Nuclear and New Energy Technology, Tsinghua University, Beijing 100084, China
[4]China Institute for Radiation Protection, Taiyuan 030012, China
[5]Northwest Institute of Nuclear Technology, Xi'an 710024, China
*Corresponding author: xuqiangxmu@hotmail.com

Received 21 October 2020; revised 3 January 2021; accepted 8 January 2021; posted 12 January 2021 (Doc. ID 412959); published 22 February 2021

Bulk scintillators that are with high density, low cost, and fine pulse-height energy spectral resolution, and are non-hygroscopic and user friendly, are desired for high-energy gamma-ray spectroscopy application. Recently, low-cost solution-processed perovskite nanoscintillators have been demonstrated with outstanding performances for indirect low-energy X-ray detection; however, the stability and thickness are not suitable for high-energy gamma-ray detection. Here, we report scintillation performances of a low-cost solution-processed bulk 0D $Cs_3Cu_2I_5$ single crystal. The self-trapped exciton emission results in a large Stokes shift (109 nm) that is reabsorption free. A broad X-ray excited emission matches well with the sensitivity of a silicon photodiode. The unique Cs^+ surrounded isolated $[Cu_2I_5]^{3-}$ cluster scintillator provides ultra-stability in air and strong radiation hardness under high-dose gamma-ray exposure from a ^{60}Co source. This solution-processed $Cs_3Cu_2I_5$ scintillator is expected with low-cost and has detection performances comparable to commercial alkali-halide scintillator products.

https://doi.org/10.1364/PRJ.412959

1. INTRODUCTION

The scintillator is a luminescence material that absorbs the energy of invisible high-energy radiation and emits UV-visible photons, and has been widely used for medical imaging, nondestructive testing, home security, and scientific research [1–5]. For high-energy photon detection, the absorption energy is strongly dependent on the density, atomic number, and atomic mass, and therefore, the scintillator is expected to have a high Z component.

During the past decades, a series of inorganic materials (such as NaI, CsI, BGO, BaF_2) has been used for gamma-ray detection [6,7]. Among them, alkali-halide scintillators [NaI(Tl), CsI(Tl or Na), SrI_2] have achieved great success for commercial applications. NaI(Tl) crystals have a high light output, and emission photons match well with the sensitivity curve of photomultiplier tubes (PMTs) with bialkali photocathodes [8]. CsI crystals have a high density for high gamma-ray stopping power [9]. The physical properties of CsI crystals are dependent on the activator: the emission peak of CsI(Na) crystal at 420 nm matches well with a bialkali photomultiplier; the emission peak of CsI(Tl) crystal at 550 nm is suitable for photodiode readout. However, several issues limit the applications: (1) high cost: growing these crystals is usually done with the Bridgman method, which requires a highly expensive furnace; (2) small Stokes shift, which causes overlapping between light emission and absorption; and (3) stability: these crystals are highly hygroscopic, which is less user friendly [10].

Recently, due to the tunable emission wavelength, high photoluminescence quantum yield (PLQY), and easy synthesis, a series of halide perovskite nanocrystals has been used for X-ray detection [11–15]. These low-dimensional nanoscintillators are ultrasensitive to low-energy X-ray photons with a low detection limit, which can be beneficial for X-ray imaging [16–18]. However, they are not thick enough for high-energy gamma-ray spectroscopy applications. Therefore, a bulk scintillator with low-cost, high-stability, no reabsorption, fine energy resolution, and user friendliness, is urgently needed [19,20]. Recently, a reabsorption-free 0D $Cs_3Cu_2I_5$ perovskite single crystal with large stopping power was used for gamma-ray detection; however, researchers now are focusing on the high-cost melt growth method [21,22].

Here, we address the issues (high cost, being hygroscopic, user friendliness, self-absorption) for both bulk and alkali-halide nanoscintillators by developing a bulk $Cs_3Cu_2I_5$ single crystal scintillator using the solution growth method with excellent features such as low cost, large stopping power, high stability, and being reabsorption free. We synthesize the bulk $Cs_3Cu_2I_5$ single crystal using a simple solution-processed method with the highest temperature lower than 85°C. Its unique Cs^+ surrounded isolated $[Cu_2I_5]^{3-}$ clusters 0D structure corresponds to remarkable stability under various atmospheres. The self-trapped exciton (STE) emission mechanism ascribes to the high PLQY (93.5%, excited with 326 nm laser) at room temperature and large Stokes shift from the absorption spectra. Our results demonstrate that the unique properties of 0D $Cs_3Cu_2I_5$ single crystal provide a wide scintillation application, especially for high-energy gamma-ray spectroscopy, which requires a scintillator with features such as low cost and being reabsorption free and user friendly.

2. EXPERIMENT

Dimethyl sulfoxide (DMSO), dimethylformamide (DMF), CsI (99.9%), and CuI (99.5%) were purchased from Aladdin. All chemicals were used without further purification. CsI (0.06 mol) and CuI (0.04 mol) were dissolved in DMSO (12 mL) and DMF (8 mL) solvent at 55°C with continuous stirring for 8 h, yielding a black solution. This solution was filtered with a 5 μm polytetrafluoroethylene (PTFE) filter, and gradually heated to 80°C with 1°C/h. Then, the crystal was harvested from the bottom of the vial. Finally, a clear and transparent crystal was obtained after it was washed with DMSO and DMF.

Powder X-ray diffraction (XRD) patterns were recorded by Panalytical X'pert PRO with a Cu-Kα radiation source. X-ray photoelectron spectroscopy (XPS) was performed on a Kratos Axis ULTRA DLD XPS system with a monochromatic Al Kα source ($h\nu = 1486.6$ eV). Optical absorption spectra were measured by a UV-Vis spectrophotometer (Shimadzu UV-2550 spectrometer) at the wavelength of 300–700 nm. Photoluminescence (PL) emission, PL decay time, and PLQY were investigated on a fluorescence spectrometer (FLS 980, Edinburg Instrument) using a xenon lamp. X-ray excited luminescence (XEL) spectra were excited by an X-ray tube with an Ag target and collected using a portable spectrometer.

Pulse height spectra were measured with an analog system, which consists of a PMT (Hamamatsu R11265U_H11934_TPMH1336E), a preamplifier (Cake 611), and a multichannel analyzer. The crystal was coupled on the window of PMT with optical silicone oil and then wrapped with Teflon. Scintillation decay time consisted of a pulsed X-ray source (XRS-3, pulse width: 25 ns), fast photodetector (GD40, without internal gain), and digital oscilloscope (Tektronix model MSO71254C). The radiation stability of the crystal was measured utilizing a ^{60}Co source at Nanjing University of Aeronautics and Astronautics. The dose rate was about 0.52 kGy/h, which was calibrated by dosimetry. All measurements were carried out in a dark atmosphere at room temperature.

3. RESULTS AND DISCUSSION

Bulk $Cs_3Cu_2I_5$ single crystal was synthesized using a simple solution-processed method. Raw commercial CsI and CuI products were dissolved into a DMSO and DMF mixture solvent with continuous stirring for 8 h. After gradually increasing the temperature by 1°C/h, the bulk crystal was harvested from the saturated solution. The crystal structure was characterized by powder XRD, as shown in Fig. 1(a). All peaks are well matched with the orthorhombic structural $Cs_3Cu_2I_5$ in space group *Pbnm* [23]. The 0D structure of $Cs_3Cu_2I_5$ is the Cs^+ cations surrounded isolated $[Cu_2I_5]^{3-}$ clusters. This unique structure is different from cubic crystal such as NaI and CsI [Fig. 1(b)]. The 0D structure exhibits strong quantum confinement and site isolation, which contribute to its remarkable and useful properties [24]. XPS was employed to analyze the chemical composition of the crystal [Fig. 1(c)]. Peaks assigned to I 3d, Cs 3d, and Cu 2p are observed. The chemical composition of the product is also taken from the XPS spectra. The measured molar ratio of Cs:Cu:I is about 3.37:2:5.6. High-resolution XPS data of the Cu, Cs, and I are collected [Figs. 1(d)–1(f)]. The broad Cu $2p_{3/2}$ peak is well fitted with two Gaussian equations, with binding energy at 931.2 eV and 932.6 eV. These two components are ascribed to the existence of both a tetrahedral site and a trigonal site of Cu^+ in the crystal. Peaks centered at 738.5 eV and 724.5 eV are ascribed to Cs $3d_{5/2}$ and Cs $3d_{3/2}$, respectively; peaks located at 619.2 eV and 930.8 eV corresponded to I $3d_{5/2}$ and I $3d_{3/2}$, respectively [23,25].

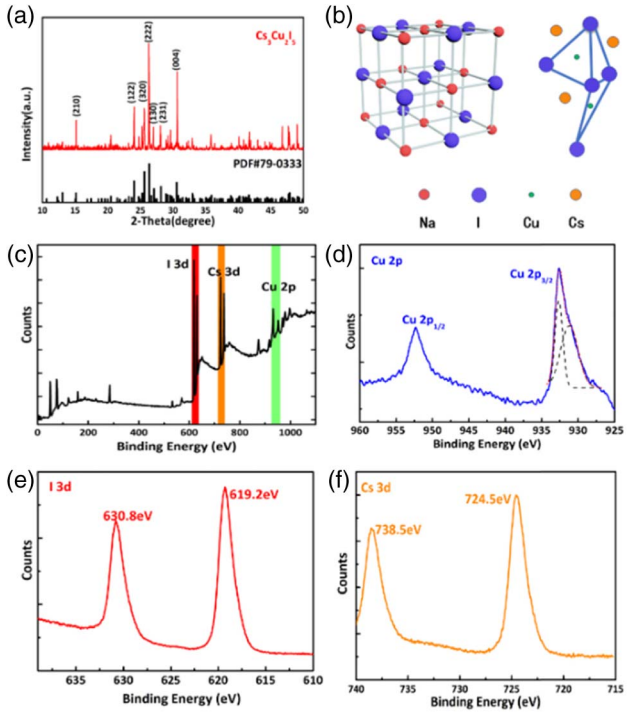

Fig. 1. (a) Powder XRD pattern of $Cs_3Cu_2I_5$. (b) Crystal structure of NaI and $Cs_3Cu_2I_5$. (c) XPS survey spectrum of $Cs_3Cu_2I_5$ SC. (d)–(f) High-resolution XPS spectra of Cu 2p, I 3d, and Cs 3d, respectively.

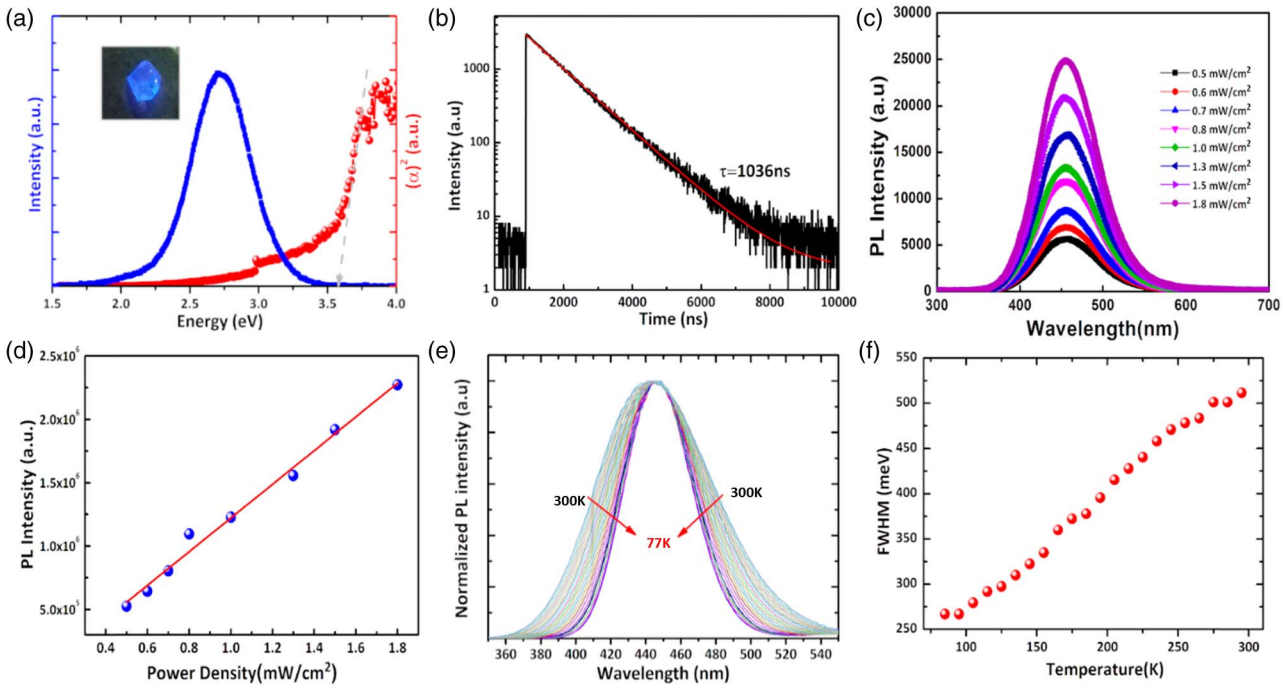

Fig. 2. Optical properties. (a) Optical absorption spectra and PL spectra of $Cs_3Cu_2I_5$ single crystal. Inset: photograph of crystal irradiated by 266 nm UV light. (b) Time-resolved PL decay of $Cs_3Cu_2I_5$ single crystal (310 nm laser excitation). (c) PL spectra excited with various power densities of 266 nm UV light. (d) Normalized temperature-dependent PL spectrum from 77 to 300 K. (e) Integrated PL intensity as a function of excited power density (266 nm). (f) FWHM of PL versus temperature from 85 to 295 K.

$Cs_3Cu_2I_5$ crystal emits strong blue light when irradiated by UV photons as shown in the inset in Fig. 2(a). A broad PL peak centered at 455 nm with full width at half maximum (FWHM) of 84 nm is shown in Fig. 2(a). Note that the PLQY of $Cs_3Cu_2I_5$ crystal is up to 93.5%, which is much higher than that of the perovskite nanocrystals [26,27]. A sharp absorption edge at the wavelength of 346 nm with a calculated optical bandgap at 3.58 eV is observed. A large Stokes shift of about 109 nm is confirmed in Fig. 2(a), which is consistent with a previous observation [26,27]. This self-absorption-free behavior can be greatly beneficial for high-energy gamma-ray detection, which requires crystals with large dimensions to attenuate high-energy gamma rays. The time-resolved PL decay of the $Cs_3Cu_2I_5$ single crystal can be well fitted with a single exponential function [Fig. 2(b)], giving the PL decay time of about 1 μs. The above PL properties (broad peak, remarkable large Stokes shift, long decay time) of hybrid metal halide–perovskite materials are attributed to the STE recombination mechanism [28,29].

We measured the PL intensity as a function of excitation intensity [Fig. 2(c)]. The integrated PL intensity exhibits a linear relationship with the excitation intensity [Fig. 2(d)]. Because the concentration of defects is finite, this linear relationship phenomenon confirms the light emission originates from STEs rather than defects.

We also investigated normalized temperature-dependent PL spectra [Fig. 2(e)]. The FWHM value decreases with the temperature from 511.5 meV at 295 K to 266.9 meV at 85 K [Fig. 2(f)], which indicates that the electron–phonon coupling capability has significantly decreased at a low temperature [30]. This electron–phonon coupling behavior is characterized by the Huang–Rhys factor (S) and phonon frequency ($\hbar\omega_{\text{photon}}$), which can be calculated with the following equation:

$$\text{FWHM} = 2.36\sqrt{S}\hbar\omega_{\text{photon}}\sqrt{\coth\frac{\hbar\omega_{\text{photon}}}{2k_BT}},$$

where k_B is the Boltzmann constant, and T is temperature. The fitted S and $\hbar\omega_{\text{photon}}$ are 54.2 and 32.3 meV, respectively. These values are slightly higher than for perovskite nanocrystals [27,31,32]. It is worth noting that the value of S is also higher than that of the reported alkali-halide scintillator (NaI of 42; CsI of 12) [33,34], and it is comparable to the recently reported defect halide perovskites ($Cs_3Sb_2I_9$, $Rb_3Sb_2I_9$, and $Cs_3Bi_2I_9$) [35].

The excellent optical properties such as high PLQY and being reabsorption free indicate it is a promising luminescence material. The calculated absorption coefficient (α) of $Cs_3Cu_2I_5$, NaI, and CsI is shown in Fig. 3(a) [36], which is correlated with the effective atomic number Z_{eff} ($\alpha \propto \rho Z_{\text{eff}}^4/E^3$), where ρ is the density and E is the photon energy. Due to the existence of heavy elements, $Cs_3Cu_2I_5$ single crystal has a high density of 4.52 g/cm^3, which results in high stopping power for high-energy photons. Under X-ray irradiation (X-ray tube with Ag target, operation voltage at 45 kV), a bright blue light is emitted from the crystal. XEL spectra as a function of X-ray dose rate are plotted in

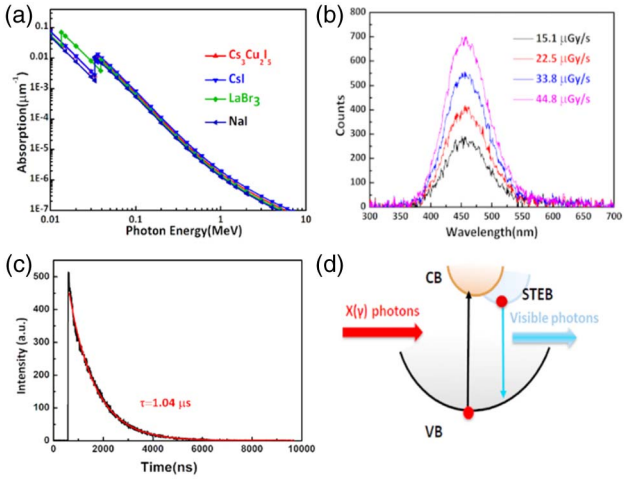

Fig. 3. (a) Theoretical calculated absorption spectra of $Cs_3Cu_2I_5$, CsI, $LaBr_3$, and NaI versus photon energy from 1 keV to 10 MeV. (b) X-ray excited luminescence (XEL) spectra of $Cs_3Cu_2I_5$ as a function of X-ray dose rate. The excited X-ray uses X-ray tube with Ag target, operated at 45 kV. (c) XEL decay profile of $Cs_3Cu_2I_5$. (d) Schematic diagram of a band model scintillation mechanism of $Cs_3Cu_2I_5$. VB, valence band; CB, conduction band; STEB, self-trapped exciton (STE) band.

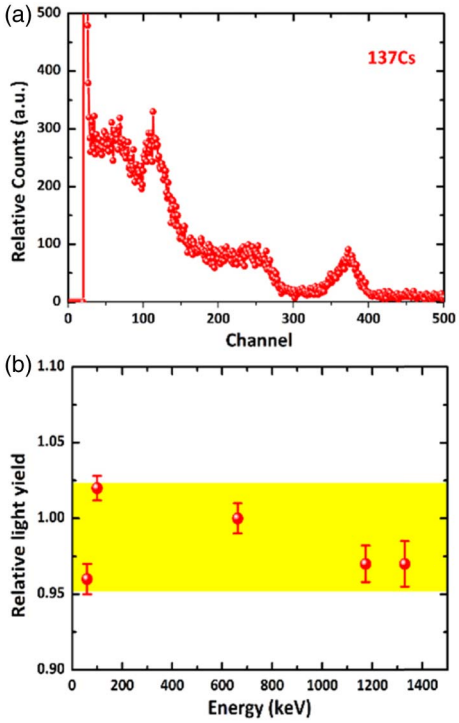

Fig. 4. (a) Pulse height spectra of 662 keV gamma-ray from ^{137}Cs radiation source. (b) Relative light yield as a function of gamma-ray energy.

Fig. 3(a). The XEL peak is located at 457 nm with FWHM of 83 nm and is well fitted with a single Gaussian equation. The room temperature scintillation decay response was studied with a pulsed X-ray system and recorded with an oscilloscope [Fig. 3(c)]. The decay time of bulk $Cs_3Cu_2I_5$ SC is 1 μs after fitting with a single exponential function, which is the same as CsI(Tl) [9]. $Cs_3Cu_2I_5$ SC shows the same light emission (emission peak, decay time) under UV photons and X-ray photons, demonstrating that the light emission mechanism is attributed to STEs. After absorbing the energy of incident X-ray photons, electrons are excited from the ground state to the excited state. Due to the strong electron–phonon coupling, the excitons are immediately transited to the STE band, and then emitted scintillation visible photons with large Stokes shift and micro-second decay time [35,37].

Pulse height spectra were successfully collected with 5 mm × 5 mm × 2 mm $Cs_3Cu_2I_5$ SC at room temperature. The crystal was covered with Teflon tape and irradiated with 662 keV gamma rays from a ^{137}Cs radiation source (1.32 μCi). The calculated energy resolution (defined as $\Delta E_{FWHM}/E$, where ΔE_{FWHM} is the photopeak's FWHM) is about 9.1% at 662 keV, which is comparable to alkali-halide commercial scintillator products. Energy resolution is given by the following equation [38,39]:

$$\left(\frac{\Delta E_{FWHM}}{E}\right)^2 = R_{stat}^2 + R_{Intr}^2 + R_{Tran}^2 + R_{Noise}^2,$$

where R_{stat}^2 is the contribution to the statistics in the number of photoelectrons. R_{Intr}^2 is correlated with the nonproportionality in the scintillation light yield with gamma-ray or electron energy. R_{Tran}^2 is associated with the inhomogeneities or nonuniformities in the scintillator, the light reflector, or the photon detector. R_{Noise}^2 is the contribution from electronic noise and variance in the gain of the photodetector. Relative light yield as a function of gamma-ray energy is recorded under excitation by ^{241}Am (60 keV), ^{137}Cs (662 keV), and ^{60}Co (1.17 MeV and 1.33 MeV), as shown in Fig. 4(b). The normalized relative light yield (normalized to that at 662 keV) of $Cs_3Cu_2I_5$ exhibits a good linear relationship with non-proportionality of 5% in the range of 60 keV to 1.33 MeV. This value is much smaller than 20% for scintillators such as NaI(Tl) or CsI(Tl). The higher proportionality is one of the important reasons for degradation in energy resolution [39]. Based on the above discussion, energy resolution could be further improved by several strategies such as enhancing the coupling between the crystal and photodetector, or reducing electronics noise. Furthermore, the light yield of $Cs_3Cu_2I_5$ is estimated by using commercial scintillators as references, which is about 31% of NaI(Tl) and 22% of CsI(Tl). The relative light yield (normalized to that at 662 keV) of $Cs_3Cu_2I_5$ in the gamma-ray energy range of 60–1275 keV is shown in Fig. 4(b). This STE-induced high scintillation performance is also observed in $Cs_2Ag_{0.6}Na_{0.4}In_{1-y}Bi_yCl_6$ nontoxic double perovskite and $Cs_3Cu_2I_5$ scintillators grown by the melt growth method [22,40]. Due to the wide bandgap of $Cs_3Cu_2I_5$, it exhibits an excellent non-proportionality, which could provide a possibility for fine energy resolution.

Stability to moisture and gamma-ray irradiation is a major concern for commercial applications. We tested the stability of $Cs_3Cu_2I_5$ crystal under a moist atmosphere and high-dose gamma-ray irradiation. The XEL spectra of the $Cs_3Cu_2I_5$ crystal irradiated by various doses of gamma rays (^{60}Co) are shown

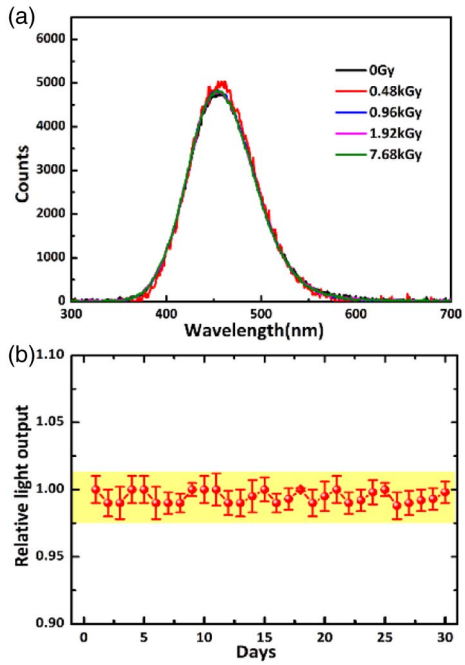

Fig. 5. (a) XEL spectra of $Cs_3Cu_2I_5$ crystal after irradiation with different doses of gamma rays from ^{60}Co. (b) Relative output of bulk $Cs_3Cu_2I_5$ crystal stored in air at room temperature for 30 days.

in Fig. 5(a). The crystals exhibit remarkable stability after exposure to a high-dose gamma ray with a radiation dose of 7.68 kGy, which are much more stable than organohalide lead perovskites [41]. Note that the scintillation output degradation under gamma-ray exposure is observed for most inorganic scintillators including BaF_2, BGO, CeF_3, and pure CsI with a dose of 340 Mrad [42]. Moisture-induced performance degradation is one of the most critical issues for perovskite commercial applications, especially for lead halide perovskite [43,44]. We put the crystal into ambient humidity at room temperature with humidity in the range of 45%–65% and measured the XEL once a day for 30 days. The normalized relative light output remained stable without degradation, as shown in Fig. 5(b). NaI and CsI scintillators are highly hygroscopic and must be hermetically packaged for use. This remarkable stability is ascribed to the unique Cs^+ surrounded $[Cu_2I_5]^{3-}$ clusters 0D structure that prevents a surface water reaction [21,26]. The long-term stability provides the capability for practical and user-friendly applications.

4. CONCLUSION

In conclusion, a high-density bulk $Cs_3Cu_2I_5$ crystal was grown by a simple low-cost, solution-processed method. The crystal with unique Cs^+ surrounded isolated $[Cu_2I_5]^{3-}$ clusters 0D structure results in characteristics such as remarkable air stability with no degradation and in being non-hygroscopic. The broad emission and zero self-absorption are attributed to the recombination of STEs, which has advantages for thick scintillator applications used in high-energy gamma-ray detection. Distinguishable pulse height spectra of ^{137}Cs were successfully collected using a 5 mm × 5 mm × 2 mm crystal. We found this 0D bulk crystal has strong radiation hardness under a high-dose gamma ray of ^{60}Co. The work demonstrates that this solution-processed, low-cost, strong-radiation-hard, and user-friendly 0D bulk crystal with STE emission could be a promising scintillator for gamma-ray spectroscopy application.

Funding. National Natural Science Foundation of China (11435010, 11705090, 11875166).

Disclosures. The authors declare no conflicts of interest.

REFERENCES

1. P. Lecoq, "Development of new scintillators for medical applications," Nucl. Instrum. Methods Phys. Res. Sect. A **809**, 130–139 (2016).
2. D. Yu, P. Wang, F. Cao, J. Liu, Z. Han, B. Huang, Y. Zou, X. Xu, and H. Zeng, "Two-dimensional halide perovskite as β-ray scintillator for nuclear radiation monitoring," Nat. Commun. **11**, 3395 (2020).
3. M. J. Weber, "Inorganic scintillators: today and tomorrow," J. Lumin. **100**, 35–45 (2002).
4. Q. Xu, W. Shao, Y. Li, Z. Zhu, B. Liu, X. Ouyang, and J. Liu, "High-sensitivity X-ray imaging of a lead halide perovskite single-crystal scintillator," Opt. Lett. **45**, 355–358 (2020).
5. B. Patric, R. Moses, T. F. Sandro, M. J. Gebhard, A. N. Genesis, F. Rene, B. Markus, M. Wilhelm, L. Samuele, B. Oier, M. J. Emyr, B. J. Christoph, K. Tobias, L. Uil, and S. Oliver, "X-ray imaging with scintillator-sensitized hybrid organic photodetectors," Nat. Photonics **9**, 843–848 (2015).
6. N. Martin and Y. Akira, "A recent R&D trends in inorganic single-crystal scintillator materials for radiation detection," Adv. Opt. Mater. **3**, 463–481 (2015).
7. C. Dujardin, E. Auffray, E. Bourret-Courchesne, P. Dorenbos, P. Lecoq, M. Nikl, A. N. Vasil'ev, A. Yoshikawa, and R.-Y. Zhu, "Needs, trends, and advances in inorganic scintillators," IEEE Trans. Nucl. Sci. **65**, 1977–1997 (2018).
8. K. Yang, M. R. Peter, and O. Vladimir, "Li co-doped NaI: Tl (NaIL)—a large volume neutron-gamma scintillator with exceptional pulse shape discrimination," IEEE Trans. Nucl. Sci. **64**, 2406–2413 (2017).
9. X. Lu, S. Gridin, T. R. Williams, A. Gektin, A. Syntfeld-Kazuch, L. Swiderski, and M. Moszynski, "Energy-dependent scintillation pulse shape and proportionality of decay components for CsI:Tl: modeling with transport and rate equations," Phys. Rev. Appl. **7**, 014007 (2017).
10. N. Martin, "Scintillation detectors for X-rays," Meas. Sci. Technol. **17**, R37–R54 (2006).
11. V. Morad, S. Yevhen, Y. Sergii, B. Alexandra, S. D. Richard, and K. V. Maksym, "Disphenoidal zero-dimensional lead, tin, and germanium halides: highly emissive singlet and triplet self-trapped excitons and X-ray scintillation," J. Am. Chem. Soc. **141**, 9764–9768 (2019).
12. Q. Xu, J. Wang, W. Shao, X. Ouyang, X. Wang, X. Zhang, Y. Guo, and X. Ouyang, "A solution-processed zero-dimensional all-inorganic perovskite scintillator for high resolution gamma-ray spectroscopy detection," Nanoscale **12**, 9727–9732 (2020).
13. C. Wang, O. Volotskova, K. Liu, M. Ahmad, C. Sun, L. Xing, and W. Lin, "Synergistic assembly of heavy metal clusters and luminescent organic bridging ligands in metal–organic frameworks for highly efficient X-ray scintillation," J. Am. Chem. Soc. **136**, 6171–6174 (2014).
14. M. Gregory, L. M. Allison, S. R. Nicholas, and H.-C. zur Loye, "Observation of intense X-ray scintillation in a family of mixed anion silicates, $Cs_3RESi_4O_{10}F_2$ (RE = Y, Eu–Lu), obtained via an enhanced flux crystal growth technique," J. Am. Chem. Soc. **139**, 14743–14748 (2017).
15. Q. Chen, J. Wu, X. Ou, B. Huang, J. Almutlaq, A. A. Zhumekenov, X. Guan, S. Han, L. Liang, Z. Yi, J. Li, X. Xie, Y. Wang, Y. Li, D. Fan, D. B. L. Teh, A. H. All, O. F. Mohammed, O. M. Bakr, T. Wu, M. Bettinelli, H. Yang, W. Huang, and X. Liu, "All inorganic perovskite nanocrystal scintillators," Nature **561**, 88–93 (2018).
16. J. H. Heo, D. H. Shin, J. K. Park, D. H. Kim, S. J. Lee, and S. H. Im, "High-performance next-generation perovskite nanocrystal scintillator for nondestructive X-ray imaging," Adv. Mater. **30**, 1801743 (2018).

17. F. Cao, D. Yu, W. Ma, X. Xu, B. Cai, Y. M. Yang, S. Liu, L. He, Y. Ke, S. Lan, K. L. Choy, and H. Zeng, "Shining emitter in a stable host: design of halide perovskite scintillators for X-ray imaging from commercial concept," ACS Nano **14**, 5183–5193 (2019).
18. Y. Zhang, R. Sun, X. Ou, K. Fu, Q. Chen, Y. Ding, L. J. Xu, L. Liu, Y. Han, A. V. Malko, X. Liu, H. Yang, O. M. Bakr, H. Liu, and O. F. Mohammed, "Metal halide perovskite nanosheet for X-ray high-resolution scintillation imaging screens," ACS Nano **13**, 2520–2525 (2019).
19. M. Gandini, I. Villa, M. Beretta, C. Gotti, M. Imran, F. Carulli, E. Fantuzzi, M. Sassi, M. Zaffalon, C. Brofferio, L. Manna, L. Beverina, A. Vedda, M. Fasoli, L. Gironi, and S. Brovelli, "Efficient, fast and reabsorption-free perovskite nanocrystal-based sensitized plastic scintillators," Nat. Nanotechnol. **15**, 462–468 (2020).
20. T. J. Hajagos, C. Liu, N. J. Cherepy, and Q. Pei, "High-Z sensitized plastic scintillators: a review," Adv. Mater. **30**, 1706956 (2018).
21. D. Yuan, "Air-stable bulk halide single crystal scintillator $Cs_3Cu_2I_5$ by melt growth: intrinsic and Tl-doped with high light yield," ACS Appl. Mater. Interface **12**, 38333–38340 (2020).
22. S. Cheng, A. Beitlerova, R. Kucerkova, M. Nikl, G. Ren, and Y. Wu, "Zero-dimensional $Cs_3Cu_2I_5$ perovskite single crystal as sensitive X-ray and γ-ray scintillator," Phys. Status Solidi RRL **14**, 2000374 (2020).
23. T. Jun, K. Sim, S. Iimura, M. Sasase, H. Kamioka, J. Kim, and H. Hosono, "Lead-free highly efficient blue-emitting $Cs_3Cu_2I_5$ with 0D electronic structure," Adv. Mater. **30**, 1804547 (2018).
24. H. Lin, C. Zhou, Y. Tian, T. Siegrist, and B. Ma, "Low-dimensional organometal halide perovskites," ACS Energy Lett. **3**, 54–62 (2017).
25. S. Hull and P. Berastegui, "Crystal structures and ionic conductivities of ternary derivatives of the silver and copper monohalides—II: ordered phases within the $(AgX)_x$–$(MX)_{1-x}$ and $(CuX)_x$–$(MX)_{1-x}$ (M = K, Rb and Cs; X = Cl, Br and I) systems," J. Solid State Chem. **177**, 3156–3173 (2004).
26. L. Xie, B. Chen, F. Zhang, Z. Zhao, X. Wang, L. Shi, Y. Liu, L. Huang, R. Liu, B. Zou, and Y. Wang, "Highly luminescent and stable lead-free cesium copper halide perovskite powders for UV-pumped phosphor-converted light-emitting diodes," Photon. Res. **8**, 768–775 (2020).
27. L. Lian, M. Zheng, W. Zhang, L. Yin, X. Du, P. Zhang, X. Zhang, J. Gao, D. Zhang, L. Gao, G. Niu, H. Song, R. Chen, X. Lan, J. Tang, and J. Zhang, "Efficient and reabsorption-free radioluminescence in $Cs_3Cu_2I_5$ nanocrystals with self-trapped excitons," Adv. Sci. **7**, 2000195 (2020).
28. C. Zhou, H. Lin, Y. Tian, Z. Yuan, R. Clark, B. Chen, L. J. van de Burgt, J. C. Wang, Y. Zhou, K. Hanson, Q. J. Meisner, J. Neu, T. Besara, T. Siegrist, E. Lambers, P. Djurovich, and B. Ma, "Luminescent zero-dimensional organic metal halide hybrids with near-unity quantum efficiency," Chem. Sci. **9**, 586–593 (2018).
29. P. Chen, Y. Bai, M. Lyu, J. H. Yun, M. Hao, and L. Wang, "Low dimensional metal halide perovskites and hybrids," Mater. Sci. Eng. **137**, 38–65 (2019).
30. J. Zhang, Y. Yang, H. Deng, U. Farooq, X. Yang, J. Khan, J. Tang, and H. Song, "High quantum yield blue emission from lead-free inorganic antimony halide perovskite colloidal quantum dots," ACS Nano **11**, 9294–9302 (2017).
31. A. A. Lohar, A. Shinde, R. Gahlaut, A. Sagdeo, and S. Mahamuni, "Enhanced photoluminescence and stimulated emission in $CsPbCl_3$ nanocrystals at low temperature," J. Phys. Chem. C **122**, 25014–25020 (2018).
32. B. J. Moon, S. J. Kim, S. Lee, A. Lee, H. Lee, D. S. Lee, T. W. Kim, S. K. Lee, S. Bae, and S. H. Lee, "Rare-earth-element-ytterbium-substituted lead-free inorganic perovskite nanocrystals for optoelectronic applications," Adv. Mater. **31**, 1901716 (2019).
33. C. H. Leung and K. S. Song, "On the luminescence quenching of F centres in alkali halides," Solid State Commun. **33**, 907–910 (1980).
34. R. K. Dawson and D. Pooley, "F band absorption in alkali halides as a function of temperature," Phys. Status Solidi B **35**, 95–105 (1969).
35. K. M. McCall, C. C. Stoumpos, S. S. Kostina, M. G. Kanatzidi, and B. W. Wessels, "Strong electron–phonon coupling and self-trapped excitons in the defect halide perovskites $A_3M_2I_9$ (A = Cs, Rb; M = Bi, Sb)," Chem. Mater. **29**, 4129–4145 (2017).
36. M. J. Berger, J. H. Hubbell, S. M. Seltzer, J. Chang, J. S. Coursey, R. Sukumar, D. S. Zucker, and K. Olsen, "XCOM: photon cross sections database," https://www.nist.gov/pml/xcom-photon-cross-sections-database (2020).
37. M. D. Smith, B. A. Connor, and H. I. Karunadasa, "Tuning the luminescence of layered halide perovskites," Chem. Rev. **119**, 3104–3139 (2019).
38. R. Devanathan, L. R. Corrales, F. Gao, and W. J. Weber, "Signal variance in gamma-ray detectors—a review," Nucl. Instrum. Methods Phys. Res. Sect. A **565**, 637–649 (2006).
39. P. Dorenbos, J. T. M. de Haas, and C. W. E. van Eijk, "Non-proportionality in the scintillation response and the energy resolution obtainable with scintillation crystals," IEEE Trans. Nucl. Sci. **42**, 2190–2202 (1995).
40. W. Zhu, W. Ma, Y. Su, Z. Chen, X. Chen, Y. Ma, L. Bai, W. Xiao, T. Liu, H. Zhu, and X. Liu, "Low-dose real-time X-ray imaging with nontoxic double perovskite scintillators," Light Sci. Appl. **9**, 1 (2020).
41. S. Yang, Z. Xu, S. Xue, P. Kandlakunta, L. Cao, and J. Huang, "Organohalide lead perovskites: more stable than glass under gamma-ray radiation," Adv. Mater. **31**, 1805547 (2019).
42. Y. Fan, L. Zhang, and R. Y. Zhu, "Gamma-ray induced radiation damage up to 340 Mrad in various scintillation crystals," IEEE Trans. Nucl. Sci. **63**, 612–619 (2016).
43. S. Zou, Y. Liu, J. Li, C. Liu, R. Feng, F. Jiang, Y. Li, J. Song, H. Zeng, M. Hong, and X. Chen, "Stabilizing cesium lead halide perovskite lattice through Mn(II) substitution for air-stable light-emitting diodes," J. Am. Chem. Soc. **139**, 11443–11450 (2017).
44. T. A. Berhe, W. Su, C. Chen, C. Pan, J. Cheng, H. Chen, M. Tsai, L. Chen, A. A. Dubale, and B. Hwang, "Organometal halide perovskite solar cells: degradation and stability," Energy Environ. Sci. **9**, 323–356 (2016).